Reprinted from SPIE Proceedings vol.3330, Smart Structures and Materials 1998: Sensory Phenomena and Measurement Instrumentation for Smart Structures and Materials, Richard O. Claus; William B. Spillman; Eds., pp.301-314, 1998.

Truly distributed strain and temperature sensing using embedded optical fibers

Luc Thévenaz, Marc Niklès, Alexandre Fellay, Massimo Facchini, Philippe Robert

EPFL, Swiss Federal Institute of Technology
Metrology Lab
CH-1015 Lausanne, Switzerland

ABSTRACT

Long-range distributed strain and temperature measurements along an optical fiber is presented, using a novel optical sensor based on stimulated Brillouin scattering. The optical effect only depends on the fiber material, so that the bare fiber itself acts as sensing element without any special fiber processing or preparation. The sensor accuracy is ± 1°C for temperature and ± 20 με for deformation. The spatial resolution is 1 meter and the sensor range is more than 20 km. Successful monitoring of a concrete dam element has been performed using an embedded standard cabled fiber. The temperature dynamics of lake waters have been also observed by simply laying a cable over the lake bed.

Keywords: distributed sensor, optical fiber, strain sensor, temperature sensor

1. INTRODUCTION

A novel optical sensor for long-range distributed strain and temperature measurements along an optical fiber is presented, based on a nonlinear effect called stimulated Brillouin scattering. This interaction causes the coupling between optical and acoustical waves when a resonance condition is fulfilled. It turns out that the resonance condition is strain and temperature-dependent, so that determining the resonance frequency directly provides a measure of temperature or strain. Local information is obtained by using pulsed lightwaves and a classical time-of-flight technique.

The resonance frequency is an intrinsic property of the material that may be observed in any silica fiber. This is very attractive since the bare fiber itself acts as sensing element without any special fiber processing or preparation. Standard optical cables may thus be used, resulting in a low-cost sensing element that may be left in the structure.

Since the optical effect only depends on the fiber material, it is absolutely stable in time and independent of the instrument. Different measurements performed over a long-term period are thus fully comparable.

Further author information

E-mail: Luc.Thevenaz@epfl.ch Fax: +41 21 693 26 14 Homepage: http://metwww.epfl.ch/Metrology.htm

2. PHYSICAL ASPECTS

Brillouin scattering results from the scattering of light by sound waves. Thermally excited acoustic waves (acoustic phonons) produce a periodic modulation of the refractive index. Brillouin scattering occurs when light is diffracted backward on this moving grating, giving rise to frequency shifted Stokes and anti-Stokes components. This process can be stimulated when the interference of the laser light and the Stokes wave reinforces the acoustic wave through electrostriction. Since the scattered light undergoes a Doppler frequency shift, the frequency difference, called Brillouin shift ν_B, depends on the acoustic velocity and is given by

$$\nu_B = \frac{2 n V_a}{\lambda_o} \tag{1}$$

where V_a is the acoustic velocity within the fiber, n is the refractive index and λ_o the vacuum wavelength of the incident lightwave. The Brillouin shift is observed in the 12-13 GHz range around a 1300 nm wavelength and in the 10-11 GHz range at 1550 nm, mostly depending on the core doping concentration. This Brillouin shift is therefore fiber-dependent and may be seen as a fingerprint of the fiber.

For sensing purpose the effect of stimulated Brillouin scattering is observed somehow differently: two lightwaves, propagating in opposite directions within a single mode fiber and showing an optical frequency difference equal to the Brillouin shift ν_B will also similarly generate an acoustic wave through electrostriction.

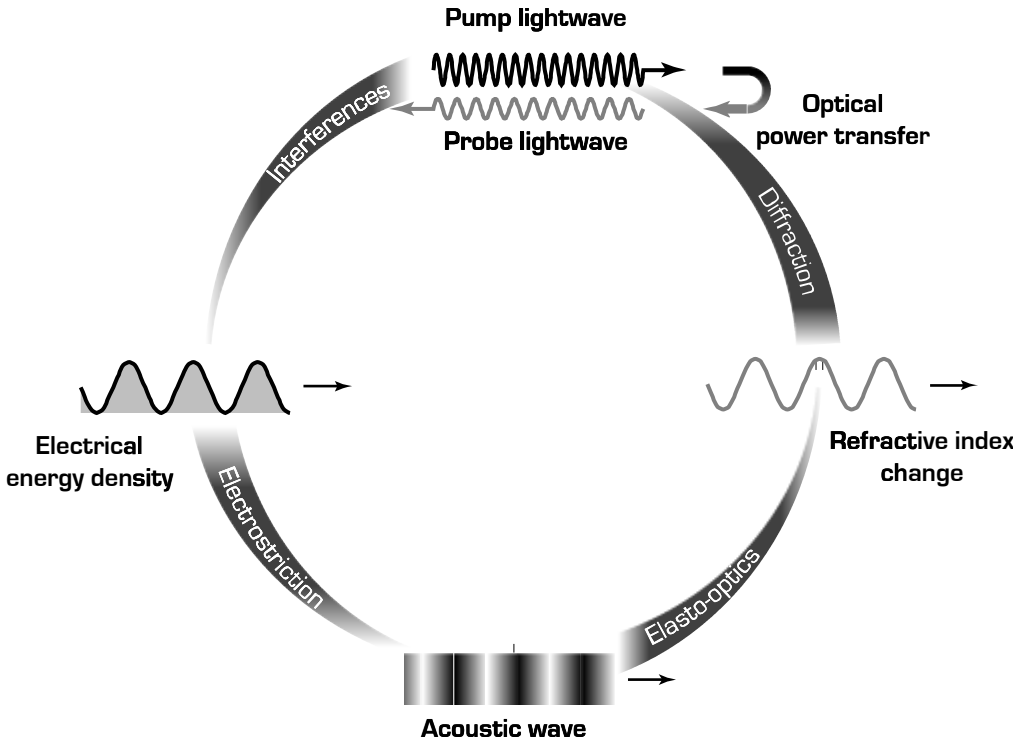

Fig. 1 Description of the stimulated Brillouin scattering. This resonant interaction involves 2 optical waves propagating in opposite directions and 1 acoustic wave and results in a power transfer from one lightwave to the other thanks to 4 different processes.

The moving grating sustained by this acoustic wave will diffract light from the upper frequency lightwave, called pump, to the lower frequency lightwave, called probe. This power transfer is equivalent to an amplification process from the probe point of view, and the net gain experienced by the probe reads:

$$I_S = I_o \, \mathrm{e}^{g_B(\nu) I_P L} \tag{2}$$

where the intensities are I_0 for the incident probe, I_S for the probe after amplification and I_P for the pump, respectively, and $g_B(\nu)$ is an equivalent gain coefficient called Brillouin gain spectrum and L the interaction length. The actual amplification experienced by the probe only depends on the pump intensity, so that the strongest effect is obtained using intense pump light, the probe power being maintained as low as possible to avoid significant pump depletion.

The strong attenuation of sound waves in silica determines the shape of the Brillouin gain spectrum. Actually, the exponential decay of the acoustic waves results in a gain $g_B(\nu)$ presenting a Lorentzian spectral profile:

$$g_B(\nu) = g_o \frac{\left(\Delta\nu_B \big/ 2\right)^2}{\left(\nu - \nu_B\right)^2 + \left(\Delta\nu_B \big/ 2\right)^2} \tag{3}$$

where $\Delta\nu_B$ is the full width at half maximum. This FWHM width ranges from 35 MHz at 1300 nm to 25 MHz at 1550 nm in standard single mode fibers, these figures being significantly increased for more special fibers.

The Brillouin gain spectrum peaks at the Brillouin frequency shift ν_B, and the peak value is given by the Brillouin gain coefficient g_o:

$$g_B(\nu_B) = g_o = \frac{2\pi n^7 p_{12}^2}{c_o \lambda_P^2 \rho_o V_a \Delta\nu_B} \tag{4}$$

where p_{12} is the longitudinal elasto-optic coefficient, ρ_o is the density, λ_p is the pump wavelength and c_o is the vacuum velocity of light.[1] In most fibers the peak gain value go lies in the $2-3\times10^{-11}\,\frac{\mathrm{m}}{\mathrm{W}}$ range.

3. EFFECT OF EXTERNAL QUANTITIES ON BRILLOUIN SHIFT

According to expression (1) the Brillouin frequency shift ν_B is directly proportional to the acoustic velocity V_a, so that any change of this velocity results in a shift of the Brillouin gain spectrum. The acoustic velocity turns out to be essentially dependent on the temperature T and the material density ρ_o, so that a variation of these quantities can be evaluated by performing a Brillouin gain spectrum measurement. The elastic properties of silica make any strain induce a volume change, resulting in a modified material density. This makes Brillouin sensing a very efficient tool for strain monitoring, either in compression or in extension, and either longitudinally or radially.

3.1 Effect of temperature

The effect of temperature on the Brillouin gain spectrum can be seen on the measurements shown in Fig. 2, performed using our experimental setup.[2] The linearity of the central frequency dependence on temperature is observed to a high confidence level over a wide temperature range, as shown in Fig. 3 (left). The slope coefficient of 1.36 MHz/°C at 1.32 µm slightly decreases for a higher GeO_2 core content. All fiber samples are only coated with a 250 µm acrylate microjacket, so that the coating influence is expected to be kept below 0.1 MHz/°C.[3]

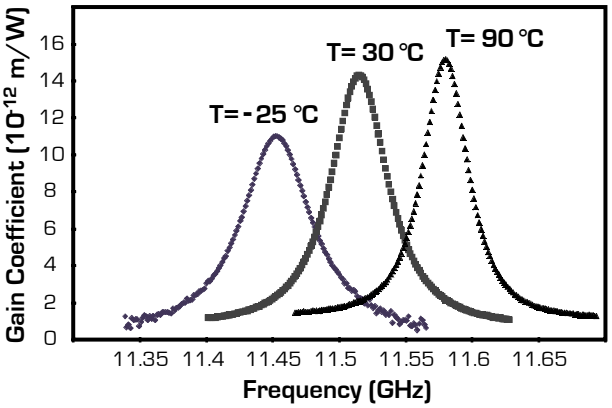

Fig. 2 Measured Brillouin gain spectra in a single mode fiber at different temperatures, showing the resonance shift and narrowing with temperature.

An interesting feature is the decrease of the Brillouin linewidth with temperature, as shown in Fig. 3 (right). The dependence is not linear and converges to a constant value at higher temperature for all fiber types. According to works performed on fused quartz samples [18], the phonon absorption peaks at a temperature close to 100 K where the Brillouin linewidth must be maximum, accordingly. The observed linewidth decrease with temperature possibly represents the upper tail of the absorption peak. The broader Brillouin gain spectrum observed at room temperature for fiber with higher GeO_2-core content is thus due to either a higher absorption peak or a higher temperature for the maximum absorption.

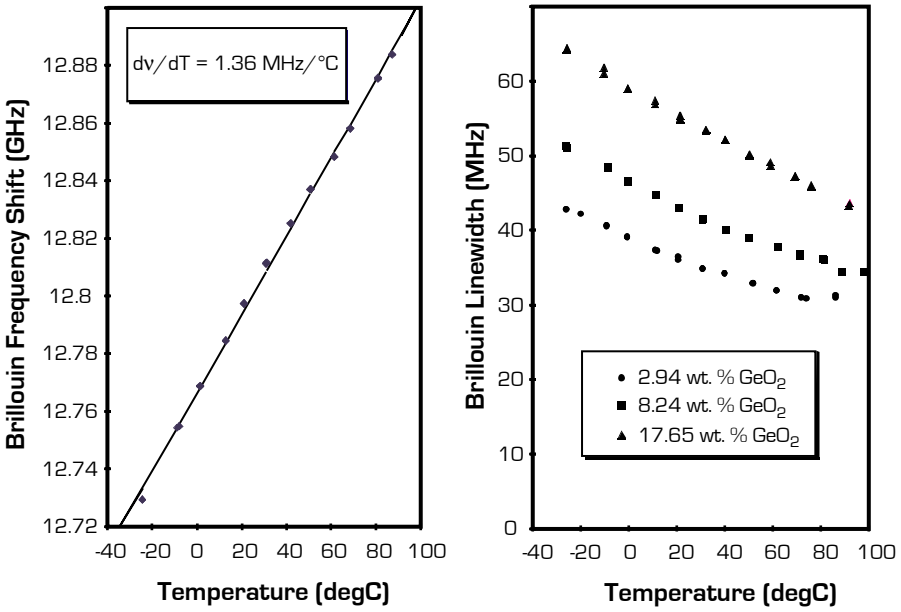

Fig. 3 Central frequency (left) and linewidth (right) of the Brillouin gain spectrum as a function of temperature. Linewidth measurements are shown for fibers with different GeO_2 core content.

The peak gain g_o increases with temperature, but the product $g_o \times \Delta\nu$ was checked to be temperature-independent, so that the Brillouin gain spectrum integrated over all frequencies remains constant. The gain increase with temperature is therefore only due to its spectral narrowing, corresponding to a smaller absorption of the phonons.

3.2 Effect of strain

As previously mentioned the acoustic velocity V_a is strain-dependent in silica fibers,[4] so that the Brillouin gain spectrum central frequency ν_B is expected to vary when the fiber is under tension. Calibrated elongation was applied to 60 m fiber samples and the Brillouin gain spectrum were measured using our instrument up to the fiber breaking point (~1% elongation).

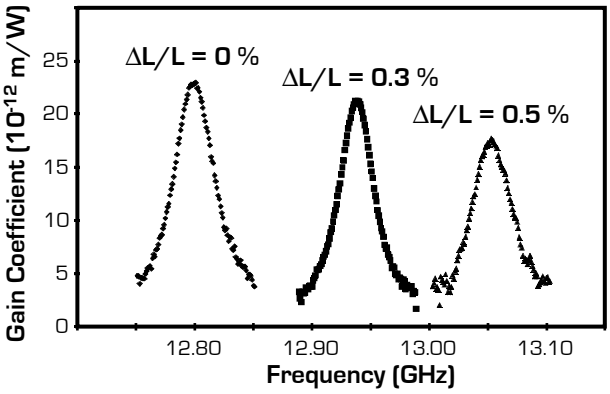

Fig. 4 Measured Brillouin gain spectra in a single mode fiberfor different fiber elongation, showing the resonance shift with strain.

The global effect of strain on Brillouin gain spectrum is shown in Fig. 4. The central frequency ν_B shows a strong dependence on strain of several tens of MHz for a 1‰ elongation. The high accuracy of the measurements performed using our instrument[3] clearly demonstrates that the linewidth $\Delta\nu$ remains unchanged with strain, while the gain g_o decreases for elongation close to the breaking point. The excellent linearity of the central frequency ν_B on strain and the invariance of the linewidth $\Delta\nu$ is confirmed in the detailed measurement shown in Fig. 5.

The central frequency experiences a shift very close to 600 MHz per percent elongation at 1.32 μm (500 MHz at 1550 nm). This coefficient was checked to be negligibly dependent on the fiber jacket type, confirming the great potentiality of Brillouin gain spectrum analysis for monitoring strains actually experienced by fibers.

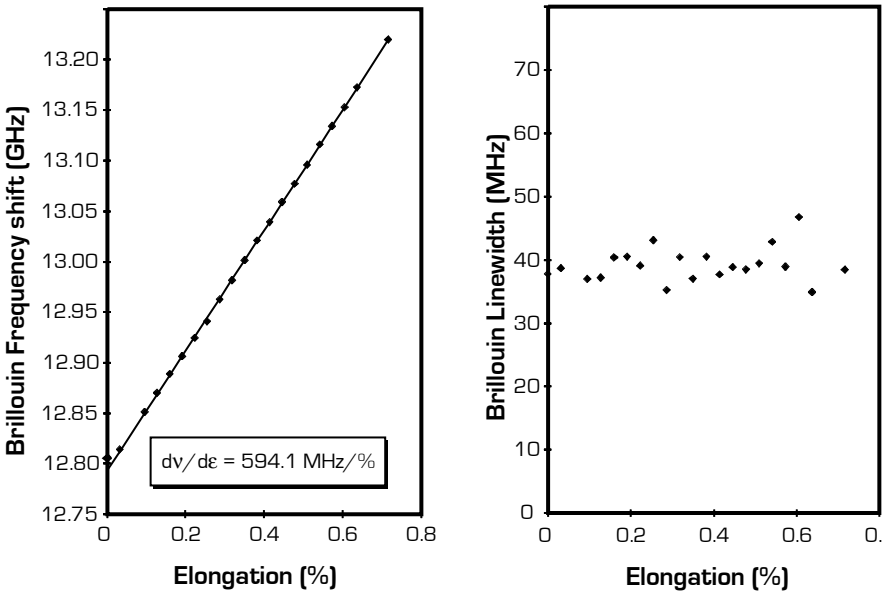

Fig.5 Central frequency (left) and linewidth (right) of the Brillouin gain spectrum as a function of elongation.

The peak gain coefficient g_o depends on many structural quantities such as material density ρ and refractive index n, that may change in a non-negligible fraction for high strain. This may explain the gain decrease for strain in the percent range. It is remarkable that the central frequency dependence on strain keeps linear under such extreme conditions.

4. DESCRIPTION OF THE INSTRUMENT

The basic configuration of a distributed Brillouin sensor is simple: a strong light pulse, corresponding to the pump, is launched into the fiber. It crosses a weak continuous (CW) lightwave, corresponding to the probe wave, that propagates in the backward direction. Stimulated Brillouin scattering occurs when pump and probe overlap, resulting in an amplification of the probe wave provided that the difference between the two frequencies lies within the Brillouin gain spectrum at the overlapping position in the fiber. As mentioned in section 2 this Brillouin gain spectrum shows a Lorentzian distribution centered on the Brillouin shift ν_B that is the quantity to determine. To obtain the Brillouin gain spectrum and thus determine ν_B, one simply measures the amplification of the probe wave while scanning its optical frequency. The local value for Brillouin amplification is obtained by a time-domain analysis like in any standard reflectometry technique.

4.1 Description of the setup

Instead of using the now traditional configuration using two laser sources,[5,6] a novel experimental configuration has been developed by our team.[7] Its main original feature is the presence of a single laser source that is modulated through a Mach-Zehnder electro-optic modulator (EOM) to generate both pump and probe lightwaves. This gives to the system an inherent stability, as far as frequency drifts of the laser are concerned. Another original feature is that pump and probe both propagate back and forth through the sensing fiber using a reflection at the far end so that the access to a single fiber end is required by the instrument. This is possible thanks to the directional property of the Brillouin gain that is only effective for contrapropagative waves, while no interaction takes place when the waves are copropagative. In other words the pump pulse provides gain to the probe signal during its forward propagation through the stimulated Brillouin scattering process while the CW probe is amplified on the way back. Only a few percent of reflection is necessary at the fiber far end, so that Fresnel reflection is actually sufficient.

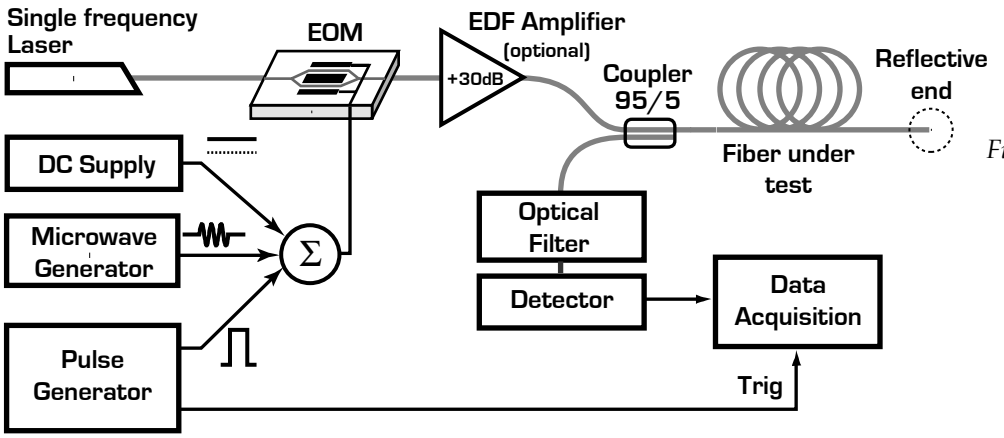

Fig. 6 Experimental setup for distributed Brillouin gain spectrum measurements, using an electro-optic modulator to generate the interacting signals.

The block diagram of the setup is shown in Fig. 6. The electro-optic modulator is the key element of the setup since it is used on the one hand for pulsing the CW light from a single frequency laser to form the pump signal, and on the other hand for the generation and frequency tuning of the probe signal. The frequency shift

on the laser light is achieved by simply applying a microwave signal on the electro-optic modulator electrodes. This creates sidebands in the laser spectrum, as shown in Fig. 7. When the modulation frequency f_m is close to the Brillouin frequency shift ν_B, the first lower sideband lies in the Brillouin gain spectrum generated by the pump and is amplified through the Brillouin interaction. As a matter of fact, the Brillouin gain spectrum can be determined by simply sweeping the modulation frequency f_m, and recording the probe intensity. The frequency spacing between the first upper and first lower sidebands is twice the frequency modulation f_m, (approximately 24 GHz), and corresponds to a wavelength separation of 0.15 nm at 1.32 µm. Inasmuch as the first upper sideband is not relevant for the measurement and even has a negative effect on the contrast, it is filtered out just before the detection using a Fabry-Perot or any narrow band filter. This technique makes the control of the probe optical frequency very convenient and reliable by adjusting the microwave modulation signal frequency. The DC bias setting on the electro-optic modulator just determines the amount of transmitted amplitude of the fundamental frequency, as can be seen in Fig. 7.

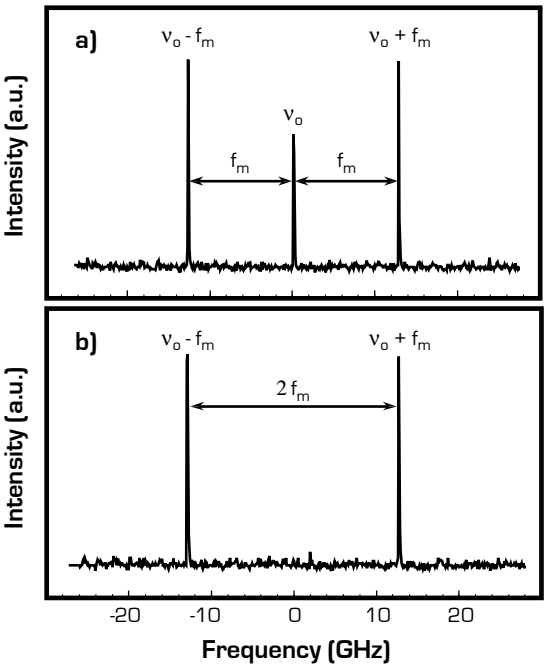

Fig. 7 Optical intensity spectra (a) of a single frequency laser modulated by an electro-optic modulator. In (b) carrier is suppressed by properly setting the DC bias on the modulator electrodes.

4.2 Performances

The spatial resolution for distributed measurements is directly related to the pulse length L. As shown in equation 2, the amplification of the probe wave exponentially decreases when L is getting shorter. This can be compensated by increasing proportionally the pump intensity, so that the product $I_P \times L$ remains constant, leaving a sufficient amplification contrast for the measurement.

On-site measurements have been first performed using a 150 mW Nd:YAG laser at 1319 nm, resulting in a 3 m best resolution. To improve this figure, it was necessary to boost the intensity of the pump wave, what can be ideally performed using an optical amplifier at 1550 nm, as shown in Fig. 6.

The erbium-doped fiber amplifier (EDFA) has a typical small-signal gain of 30 dB and a saturation output power of about 15 dBm. In pulsed regime, even an input pulse with a several mW peak power may experience the small-signal gain, provided that the average output power does not exceed the saturation power. This can be achieved by sufficiently decreasing the pulse duty cycle. Peak pump powers in the Watt range can thus be obtained. Minimal absorption loss is a further advantage of the 1550 nm transmission window, making a 100 km sensing range possible.

The spatial resolution is however subject to a more fundamental limitation: it results from the pulsed nature of the pump wave, and determines the ultimate resolution of the Brillouin sensor. In Equation 2, it was

assumed that the gain spectrum $g_B(\nu)$ does not depend on the length L of the pump pulse. This is no longer true for short pulses: the pulse optical bandwidth is no longer negligible with respect to the Brillouin gain linewidth, so that the effective Brillouin gain spectrum $\overline{g}_B(\nu)$ experienced by the signal wave is given by the convolution between the original $g_B(\nu)$ and the spectrum of the pump pulse. Assuming a perfectly rectangular pulse of width L, this convolution yields the following expression :

$$\overline{g}_B(\nu) = 2\,\mathrm{e}^{-\pi \Delta\nu_B L}\left\{\cosh(\pi\,\Delta\nu_B\,L) - \cos\left(2\pi\,(\nu-\nu_B)\,L\right)\right\}\; g_B(\nu) \qquad (5)$$

$\overline{g}_B(\nu)$ must replace the intrinsic Lorentzian spectrum $g_B(\nu)$ in equation 2 to calculate the actual amplification of the probe signal. The effective Brillouin gain spectrum spreads for shorter pulses, resulting in a drastic decrease of the peak gain, and of the measured signal consequently. In addition, this effect is detrimental for the frequency resolution of the measurements, the central frequency of such a spread distribution being determined with less accuracy.

It is possible to estimate the ultimate resolution of a distributed Brillouin sensor as a function of the fiber length : it is the minimal pulse length giving a sufficient amplification, say 2 %, when the spreading of the gain spectrum and the effect of absorption are taken into account. With our system specifications, the calculation yields the relation shown in Fig. 8. The most remarkable feature shown on this graph is the maintained resolution over a long distance: it remains below 3 meters over 50 km, as a consequence of the low loss at 1550 nm. On the other hand, the optimal resolution for short fibers (<1 km) is slightly less than 1 m. This kind of sensors is thus definitely dedicated for long range measurements with meter resolution and is not suitable for a centimeter resolution.

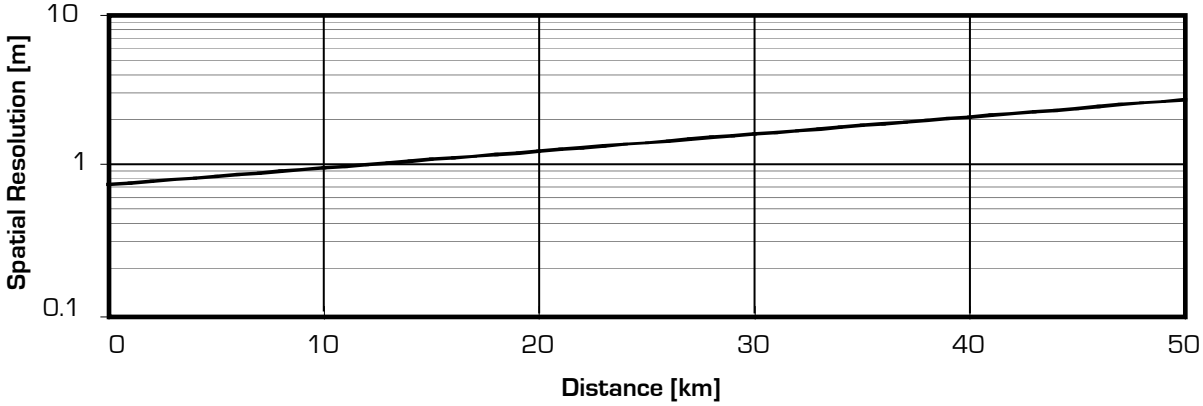

Fig. 8 Spatial resolution as a function of the distance at a wavelength of 1.55 μm in real conditions.

The accuracy on the determination of the Brillouin shift ν_B depends on the amplification contrast and the probe signal intensity. In standard fibers and for the figure of merit shown in Fig. 8 an accuracy of 1 MHz is observed. This approximately corresponds to a 1 degC temperature resolution and to a 2×10^{-5} strain resolution. The Brillouin shift accuracy can be improved to 250 kHz at the expense of a worse spatial resolution or a longer measurement time, corresponding to a 0.25 degC temperature and 5×10^{-6} strain resolutions, respectively.

5. APPLICATIONS USING THE DISTRIBUTED BRILLOUIN SENSOR

This sensor has experienced many tests for different applications, some of them being directly performed in the field. The most significant are reviewed in this section.

5.1 Strain measurement

A first simple laboratory test was performed to check the sensor resolution and reliability: a 80 cm segment of a 37 m fiber was loaded using a 155 g weight, giving rise to a stretch of the fiber resulting of its own elastic properties, as sketched in Fig. 9. The stretched segment is clearly identified in the Brillouin distributed measurement shown in Fig. 10, and the 1.52‰ measured elongation is in exact agreement with the calculated value using tabulated coefficients for silica. Such a measurement also demonstrates that a meter spatial resolution is possible, corresponding to the ultimate sensor capability.

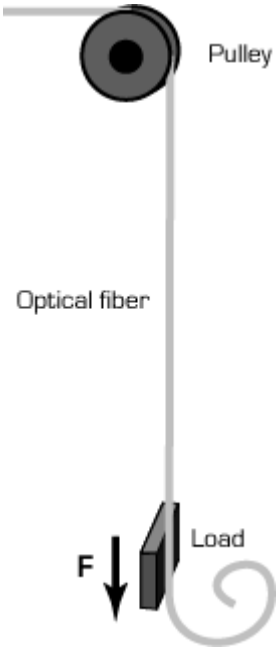

Fig. 9 Setup of a simple fiber straining experiment.

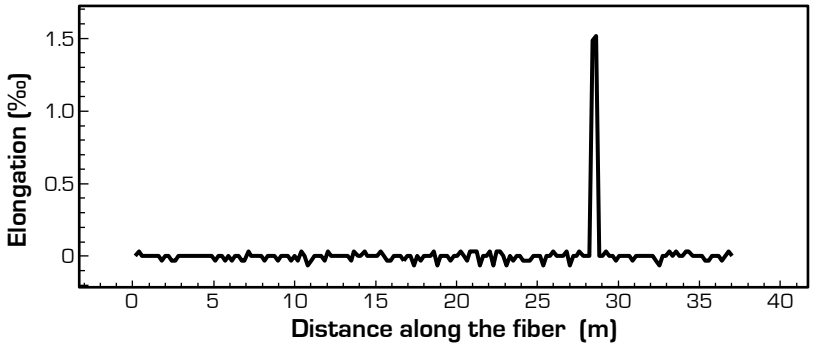

Fig. 10 Result of the straining experiment shown in Fig. 9 measured using a distributed Brillouin sensor boosted by an erbium-doped optical amplifier. The 80 cm stretched segment is clearly identified.

Another test was performed in more real conditions: a strong tensile load was applied to a telecommunication cable by mean of a pulley system, as shown in Fig. 11. This is a classical test to check the cable resistance and buffering capability regarding the fibers bundled in the cable. In particular this test is decisive to determine the critical pulling force for which the fibers start to be strained.

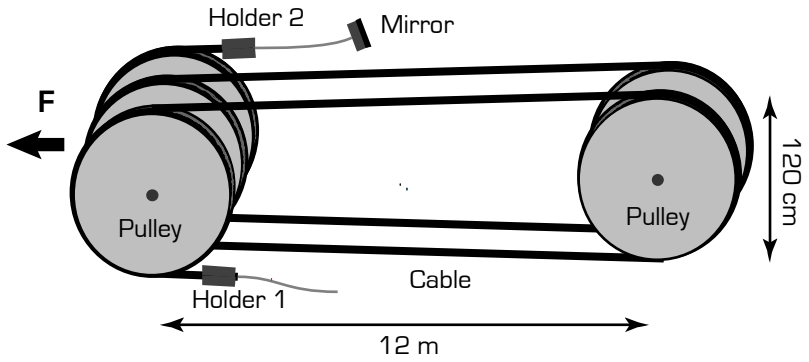

Fig. 11 Traction bench for testing the cable resistance to a tensile force. Longer cables can be checked thanks to the pulley system.

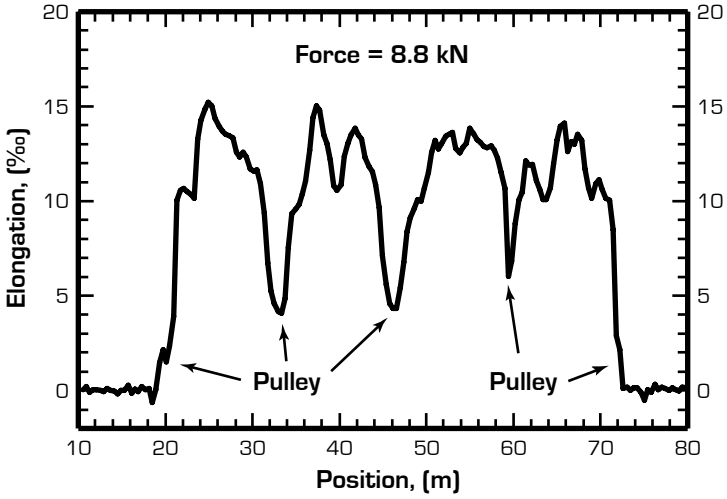

Fig. 12 Distributed measurement of the elongation of a fiber in a cable stressed by the system shown in Fig. 11.

In Fig. 12 the Brillouin distributed measurement using this pulley system shows an non-uniform fiber elongation over the cable length. The fiber is clearly less strained at the pulleys position. The total fiber elongation can be easily determined by integrating the local elongation over the entire cable length, as shown in Fig. 13 for different tensile forces. The critical pulling force is clearly observed and the linear behavior of fiber elongation for a larger applied force. This is in perfect agreement with other measurement of the total elongation, performed using a classical technique based on phase delay measurements.

This result shows that the Brillouin sensor delivers more complete information, since the local strain may differ significantly from the average strain. This is particularly important regarding the fiber breaking probability that is of course directly related to the local strain.

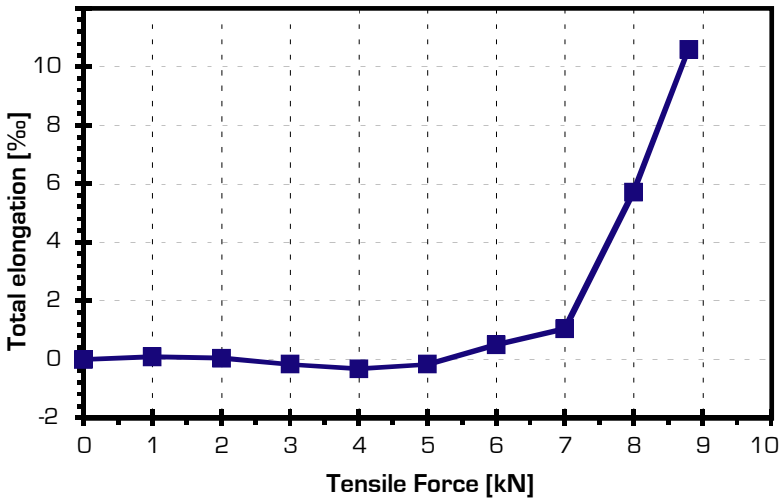

Fig. 13 Total fiber elongation over the full cable length for different tensile force, each point being calculated by integrating a measurement similar to Fig. 12.

5.2 Temperature measurement

A good application for a fiber distributed temperature sensor is the monitoring of electrical power cables to detect destructive overheating and to localize hot spots. For this purpose fibers were bundled in the screen layer of a 60 kV cable, as shown in Fig. 14, the perfect dielectric properties of the fibers making the light propagation insensitive to the extreme electromagnetic environment of such a cable. A typical temperature distribution along the cable is presented in Fig. 15, showing important variations of the local

Fig. 14 High-voltage 60kV cable with bundled fibers for temperature monitoring.

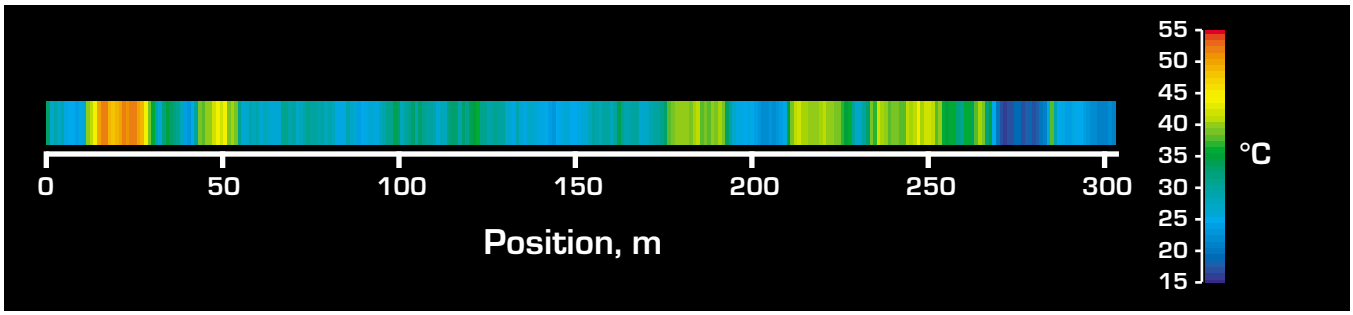

Fig. 15 *Temperature distribution along an electrical power 60kV cable, measured using the distributed Brillouin sensor with optical fibers bundled in the screen layer of the cable. The elctrical current was 130A and strong temperature fluctuations are observed mostly due to environmental conditions.*

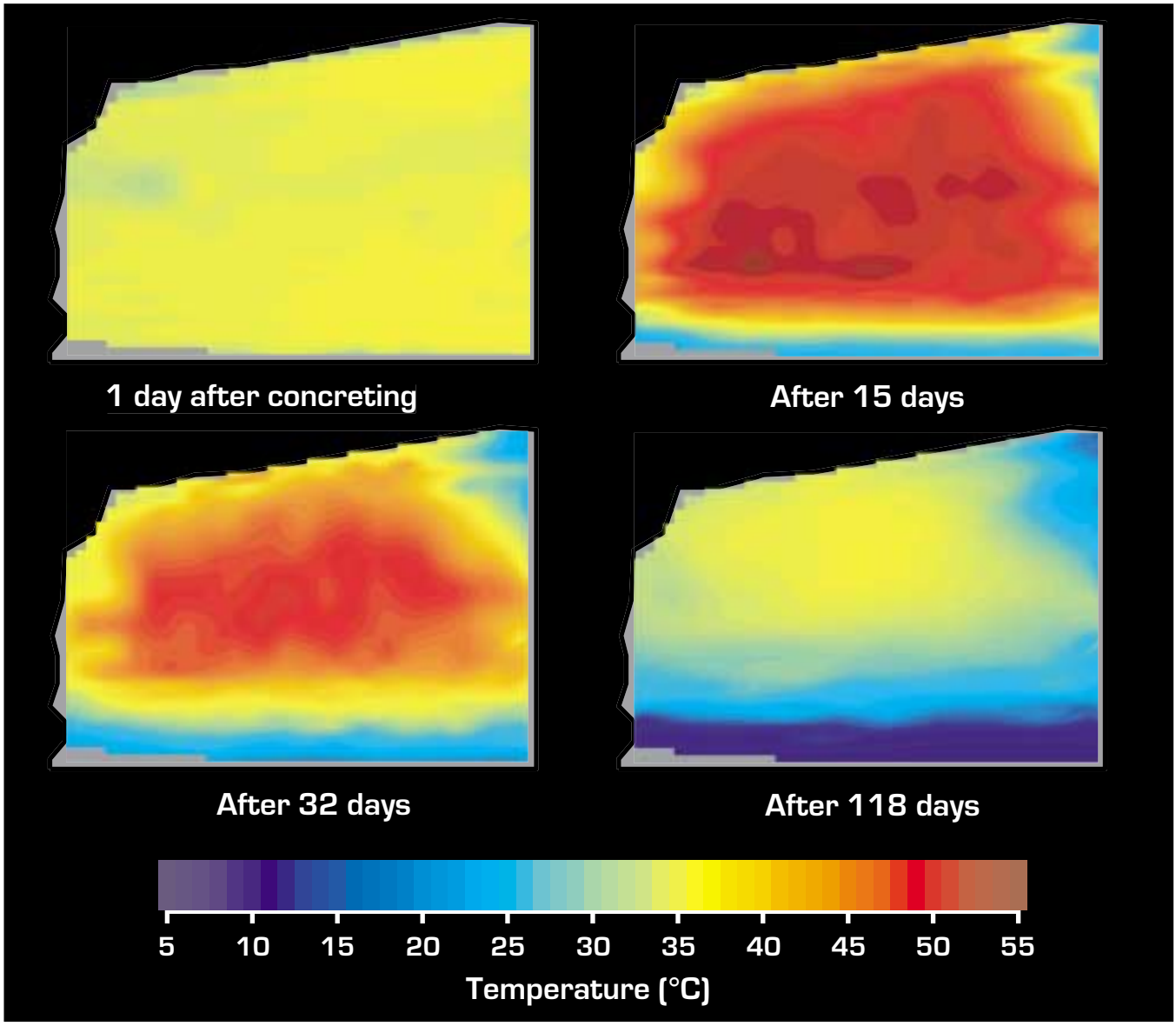

Fig. 16 *Two-dimensional temperature distribution during the setting of the concrete slab shown in Fig. 17, obtained using the distributed Brillouin sensor with an optical cable embedded within the concrete.*

temperature due to different environmental conditions, such as soil humidity and sun exposition.

Another application is the monitoring of the concrete setting temperature in civil engineering works. This monitoring is of prime importance in critical works, since the density and the importance of microcracks are directly related to the maximum temperature experienced by the concrete during the setting chemical process.

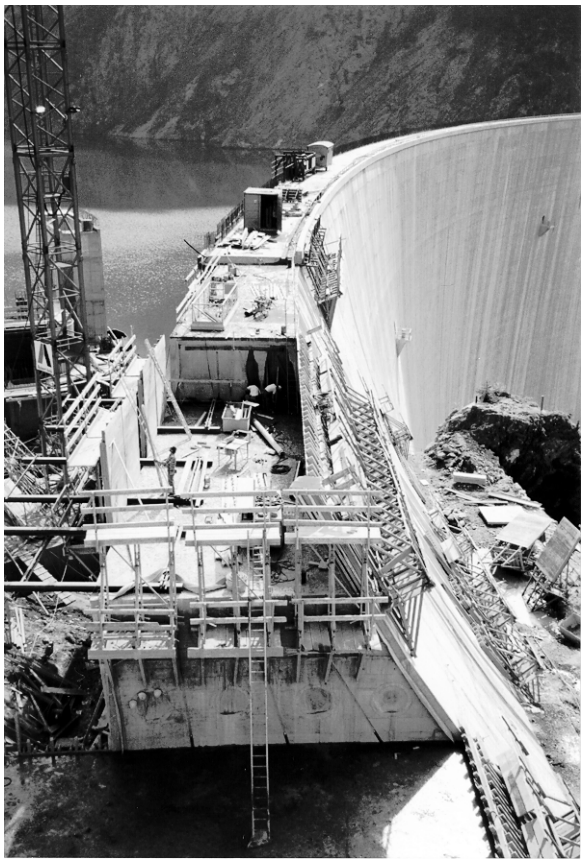

A major dam at Luzzone in the Swiss Alps was recently raised to increase the power capability of the associated hydroelectric plant. This raising was actually achieved by stacking gradually new concrete slabs of 15 m x 10 m average size for a 3 m thickness, as shown in Fig. 17. A small optical telecommunication cable was installed during the concrete pouring over the central layer of the largest slab, so that the embedded cable makes a dense horizontal mat, necessary to obtain a two-dimensional temperature distribution of the whole central slab area. Fig. 16 shows the temperature distribution over the slab at different moment after the concrete pouring. It can be clearly seen that the temperature rises up to 50 degC in the central area and that it takes many weeks to cool down this region. The outer slab areas rapidly stabilize at the ambient temperature, so that an observer is totally unaware that the concrete is still fairly hot in the central region of the dam.

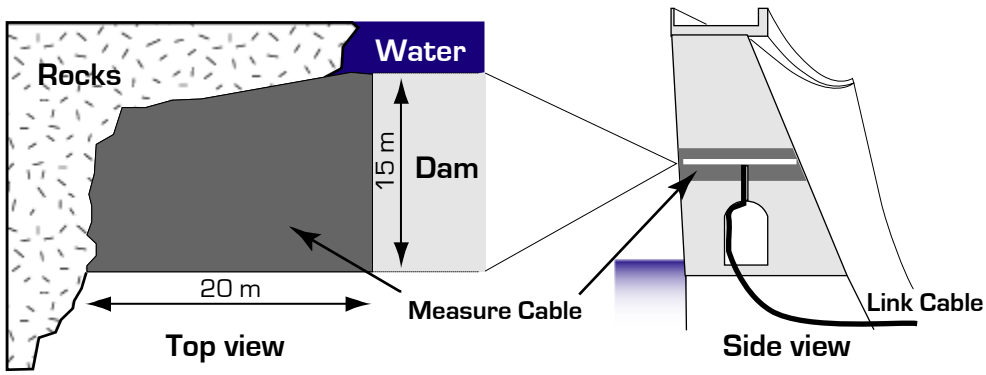

Fig 17 View of the concrete slab and of the mat-like installation of the measuring cable for concrete setting temperature monitoring, during the raising of Luzzone dam in the Swiss Alps.

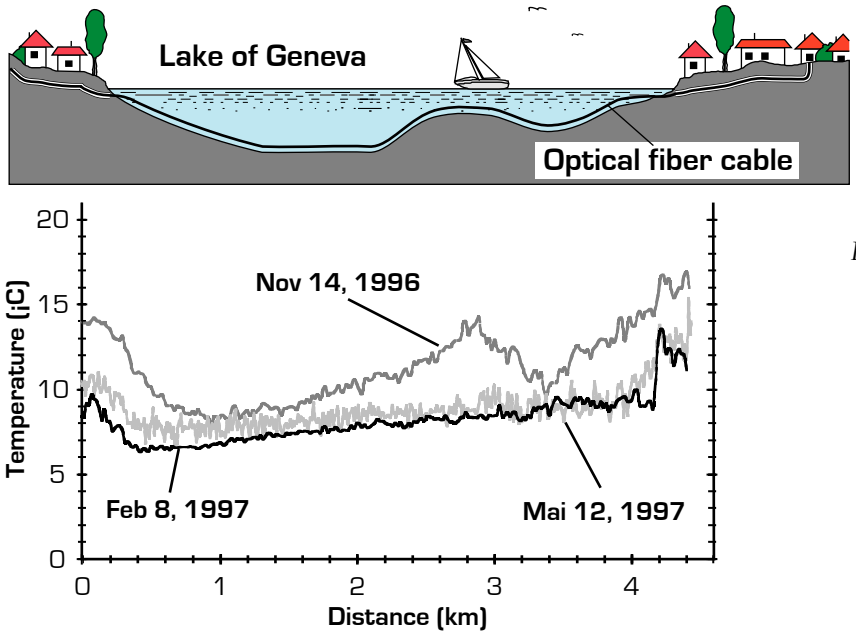

Fig. 18 Temperature profile of the water on the bed of the Lake of Geneva, Switzerland, showing significant seasonal changes in the temperature distribution.

Finally a cable installed by a telecommunication operator over the bed of the lake of Geneva in Switzerland was used to observe the temperature change of the deep waters in relation with seasonal conditions. Fig. 18 shows that the surface water moves down to the lake bed during the winter (November measurement), heating up the deep waters. This breaks the layered distribution of temperature and generates a complete water mixture essential for the lake oxygenation and the biological life, consequently.

6. CONCLUSION

Demonstrative tests of distributed temperature and strain measurements have been performed in the field using an instrument based on the local analysis of the stimulated Brillouin interaction (LASBI). This instrument is based on an original configuration using a single laser source and a pump and probe technique. In addition, access to a single fiber end is required to perform the measurements, what is an obvious advantage in the field. The nature of the Brillouin interaction makes such a sensor dedicated to long range measurements (up to 100 km) with a meter resolution. The physical limit for the spatial resolution is reached with this instrument and improvements are now rather expected in the temperature and strain resolution and in the acquisition time, that is currently 3 minutes for 1024 points.

Another problem that is often pointed out is the impossibility to discriminate between temperature and strain effect with a Brillouin shift measurement. To our opinion the problem can be in real conditions easily worked out by combining loose-tubed and tight cables. In a loose tube the fiber is granted to be unstrained and is therefore only sensitive to temperature. If strain information must be obtained a parallel tight cable must be installed that is fixed on the structure, so that the fiber can experience strain. The drawback of a double-length sensor is widely canceled out by the very long range capability of such a sensor. Only this double-length configuration may grant a maintained accuracy for temperature and strain. Other configuration using the

particularity that the Brillouin linewidth depends only on temperature and not on strain would result in an unacceptable accuracy for most applications.

7. ACKNOLEDGEMENTS

The authors are grateful to Mr P.Salina and Dr H.Gilgen from Swisscom, to Dr B.Dardel from Alcatel, to Dr A.P.Bouille from AESA and to the Swiss Electrical Energy Funding (PSEL) for their financial and technical support and for valuable discussions.

8. REFERENCES

1. G. P. Agrawal, *Nonlinear fiber optics*, Academic Press, Boston, 1989.

2. M.Niklès, L.Thévenaz, Ph.Robert, "Brillouin gain spectrum characterization in single-mode optical fibers", J. *Lightwave Technol.*, **LT-15**, pp. 1842-1851, 1997.

3. T.Kurashima, T.Horigushi, M.Tateda "Thermal effects on the Brillouin Frequency Shift in jacketed optical silica fibers", *Appl. Opt.* , **29**, p. 2219, 1990.

4. A.S.Pine, "Brillouin Scattering Study of Acoustic Attenuation in Fused Quartz", *Phys. Rev.*, **185**, p. 1187, 1969.

5. T.Horiguchi, T.Kurashima, M.Tateda, "A technique to measure distributed strain in optical fibers", *Photonics Tech. Lett.*, **2**, p. 352, 1990.

6. X. Bao, J. Dhliwayo, N. Heron, D.J. Webb, D.A. Jackson, "Experimental and theoretical studies on a distributed temperature sensor bases on Brillouin scattering", *J. Lightwave Technol.*, **13**, p. 1340, 1995.

The Brillouin distributed fiber sensor *LASBI 9800*.

7. M.Niklès, L.Thévenaz, P.Robert, "Simple distributed fiber sensor based on Brillouin gain spectrum a analysis", *Optics Lett.*, **21**, pp. 758-760, 1995.